Computers & Geosciences 82 (2015) 191–204

Contents lists available at ScienceDirect

Computers & Geosciences

journal homepage: www.elsevier.com/locate/cageo

Geometric attribute and shape characterization of modern depositional elements: A quantitative GIS method for empirical analysis

Björn Nyberg [a,b,*], Simon J. Buckley [a], John A. Howell [c], Rachel A. Nanson [d]

[a] Uni Research CIPR, P.O. Box 7810, 5020 Bergen, Norway
[b] Department of Earth Sciences, University of Bergen, P.O. Box 7803, 5020 Bergen, Norway
[c] Department of Geology and Petroleum Geology, University of Aberdeen, Meston Building, Old Aberdeen, AB24 3UE Scotland, UK
[d] Australian School of Petroleum, Centre for Tectonics, Resources and Exploration (TRaX), Santos Petroleum Engineering Building, University of Adelaide, Adelaide, SA 5005, Australia

ARTICLE INFO

Article history:
Received 13 January 2015
Received in revised form
2 June 2015
Accepted 8 June 2015
Available online 22 June 2015

ABSTRACT

The recent rise in the quality and availability of remote sensing data has benefitted the geoscience community by allowing high resolution studies of the geometry of modern clastic depositional elements, which are analogous to the elements that control fluid flow in subsurface reservoirs. Established methods used to describe the geometry of these features have been predominantly subjective. We present a new objective technique to automate the characterization of *centerline attributes* (CA) of mapped depositional elements. This technique measures key parameters at a defined sampling interval along a calculated centerline for each input shape, which are automatically analyzed to define geometric shape, length, width, sinuosity, adjacency and centerline deviation. To demonstrate the applicability of the method to a range of depositional environments, mapped sandbodies from two contrasting modern systems were analyzed: (1) the 520 km^2 mixed-process Mitchell River Delta, Gulf of Carpentaria, Australia; (2) a 1200 km reach of the anabranching Congo River, Democratic Republic of the Congo.

1696 Wave- and fluvial-derived elements from the Mitchell Delta were analyzed using our CA method and the conventional minimum bounding box (MBB) approach. The MBB results defined the regression slopes as 1.25–4.47 times wider and 0.31–0.97 times shorter than their CA values. Results applied to 2221 mid-channel bar elements in the Congo River showed similar CA and MBB relationships, with linear regression slopes of a MBB as 1.06 times wider and 0.97 times shorter. The inconsistency in the comparative MBB and CA results for these two datasets is attributed to the very different geometries of the sandbodies in these contrasting depositional environments. This suggests that caution should be exercised when applying current methods. A major benefit of the proposed CA method is that it allows quantitative study at scales and levels of detail typically not practical using manual solutions.

1. Introduction

In recent years, research and debate on quantitative global distributions of depositional environments and their importance to the preserved sedimentary record has increased within the scientific community (e.g., Stutz and Pilkey, 2002; Hartley et al., 2010; Weissmann et al., 2010; Holzweber et al., 2014) , and has been largely driven by the availability and accessibility of global, remotely sensed datasets. Google Earth (Lisle, 2006) embodies this move from isolated analogue maps and photographs to complete global coverage on a geoscientist's computer. As the trend for investigating the relational, geometric and distribution statistics of depositional environments, with focus on increasingly smaller-scale features, deriving quantitative geometric data using traditional subjective and manual methods becomes impractical and inefficient. However, such quantitative measurements are important for deriving empirical and statistically-valid relationships on the spatial variability of elements within modern depositional systems.

Quantitative measures for describing the geometric attributes of depositional elements are currently limited to standard geographical information system (GIS) operations, which do not adequately represent the length, width, sinuosity, adjacency or orientation of these units beyond basic individual maximum or minimum values. The problem of automatically and more objectively determining the shape of, and interactions between, such features has been approached by authors in numerous fields

* Corresponding author at: Uni Research CIPR, P.O. Box 7810, 5020 Bergen, Norway.
E-mail address: bjorn.burr.nyberg@gmail.com (B. Nyberg).

http://dx.doi.org/10.1016/j.cageo.2015.06.003
0098-3004/

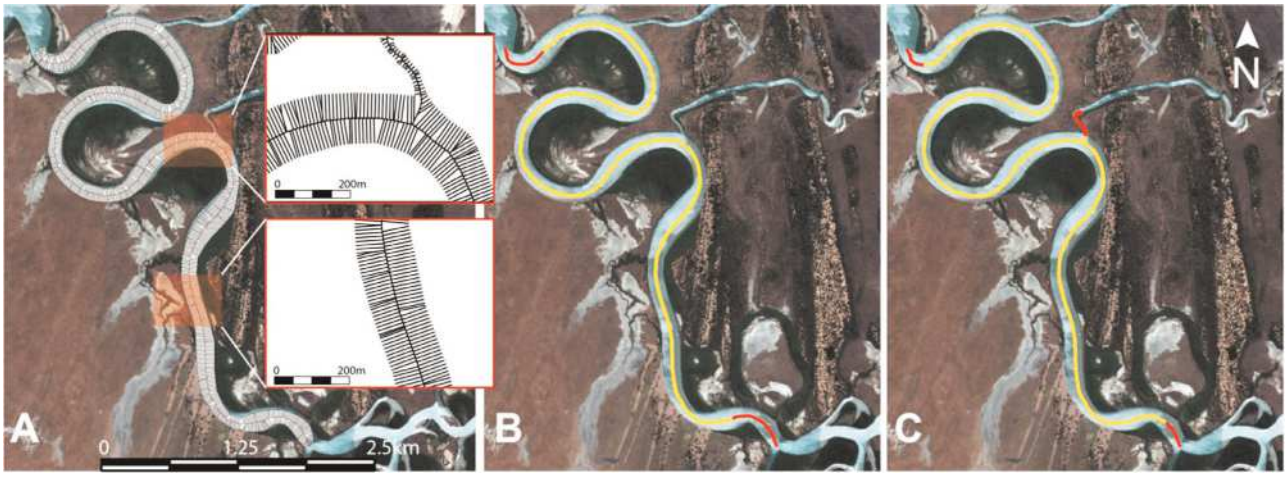

Fig. 1. (A) Overview of a small portion of a meandering channel traversing the Mitchell River delta with its skeletal lines identified by Voronoi tessellation. Inset: close ups of the high resolution line (minimum 10 m [vertex] spacing) segment mesh, with the uppermost box identifying a potential branch in channel. (B) Typical result of the pruned skeletal line (yellow) made by removing excess line segments, including the channel branch, overlain by the proposed double single source-Dijkstra method result (red). (C) Multiple (three) endpoints identified by first pruning the skeletal line (yellow) and then extending that data to the polygon edge (red). Background imagery© Bing™.(For interpretation of the references to color in this figure legend, the reader is referred to the web version of this article.)

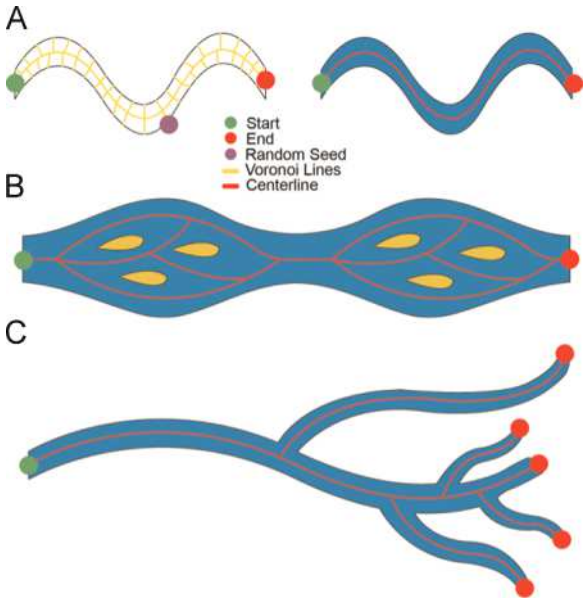

Fig. 2. Scenarios that define a centerline of any given feature. (A) Example of a random seed selection within the skeletal line that is subsequently used to define the start and end points by the double single-source Dijkstra method. (B) Centerline created with internal closed loops; (C) expansion of A and B using multiple endpoint (branch) members.

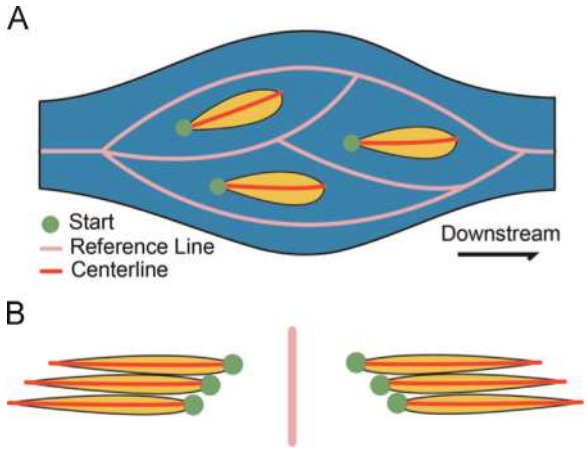

Fig. 3. If the start vertex of an individual centerline is to be correlated to the depositional system direction, the cumulative shortest distance along the reference line to each polygon is used (A). Otherwise each centerline is oriented to its closest proximity to a single reference line, as shown in (B).

(Gardoll et al., 2000; van der Werff and van der Meer, 2008; Tafesse et al., 2012; Kröner and Doménech Carbó, 2013). Object Based Image Analysis (OBIA) exemplifies the movement of combining measures of shape and geometry to improve automated image classification for the purpose of categorizing remotely sensed data with similar spectral responses (Benz et al., 2004; Blaschke, 2010). Describing shapes and geometric attributes typically relies on the definition of mathematical relationships between a feature's geometric parameters to obtain circular, rounded, elongated or rectangular classes, rather than a quantitative set of measurements to objectively define shape. The minimum bounding box (MBB) approach (e.g., Freeman and Shapira, 1975) has previously been used as a means of defining a feature's axis lengths, minimum bounding area and perimeter, compactness and convexity for this purpose.

Pavelsky and Smith (2008) and Fisher et al. (2013) have recently shown the potential for obtaining quantitative width measurements for river channel geomorphology research. Although the methodology to classify the broad spectrum of depositional environments, characterization of shape, heterogeneity and connectivity of elements is not considered that otherwise have important implications for relating modern analogue studies for subsurface reservoir modeling (Howell et al., 2008; Nanson et al., 2012; Massey et al., 2013). The MBB method remains the most accessible automated methodology for quantitative data analysis within standard GIS suites. A final consideration is that an accurate set of measurements (e.g., Holzweber et al., 2014) and shapes (e.g., Nanson et al., 2012) of modern elements can be achieved using manual interpretation. This is both time-consuming and subjective and limits the quantification of the large amounts of global data available today.

In this paper we present a centerline attribute (CA) method for the quantification of the geometric attributes of shapes that can aid geomorphologists in interpreting the heterogeneity and spatial variability of elements within modern clastic depositional systems. By describing the centerline of a mapped feature and measuring multiple equally spaced width and centerline deviation (sinuosity) measurements along that centerline, variability can be quantified

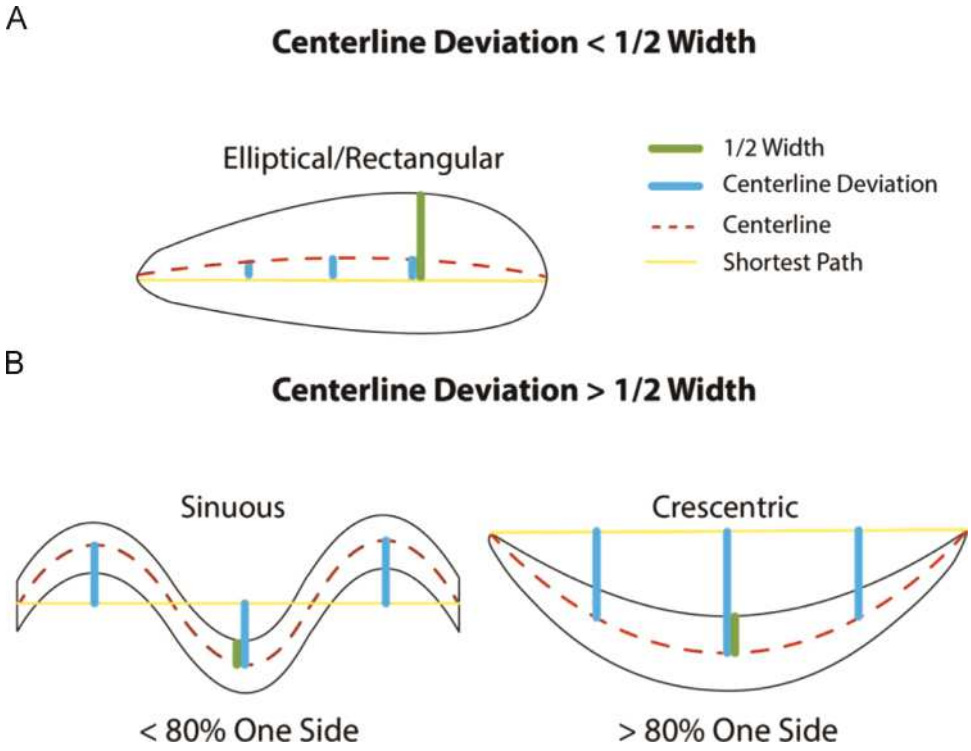

Fig. 4. (A) A sinuosity threshold determines the degree of sinuosity that may classify an ellipse or rectangular shape; (B) Proportion of the centerline deviation occurring on each side of the shortest path line defines elements as crescentic or sinuous.

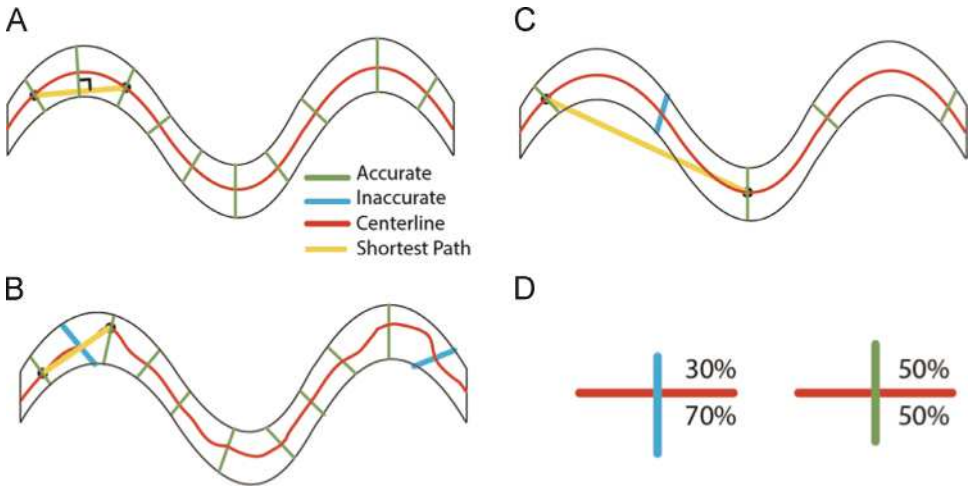

Fig. 5. Width measurements are calculated based on the line perpendicular to the shortest path, as defined between two endpoints along the centerline, and the intersection with the element boundary. High quality width measurements result from a good centerline representation and appropriate sample spacing, (A). When the centerline is poorly defined (B), or sample spacing does not reflect the centerline variation (C), low quality width measurements will result. An unreliable width measurement can be identified using the proportion of the line that occurs on either side of the centerline (D).

in terms of these centerline attributes. Furthermore these geometric attributes can aid in classifying features into one of nine geomorphological classes by describing symmetry and centerline deviation with distance. The spatial occurrence of each feature's geometric attributes in the context of a depositional system allows for further analysis to examine the adjacency of geomorphic elements, important for understanding potential reservoir connectivity. The aims of the paper are to describe the individual measurements and calculations using the proposed method and to demonstrate the applicability of the method for two case studies.

2. Method

The proposed methodologies are implemented as individual scripts running in the Quantum GIS (QGIS) environment (QGIS Development Team, 2014) and based on the integrated GRASS GIS suite (GRASS Development Team, 2014). Depending on the desired application, these scripts can be combined into automated workflows based on a number of predefined parameters, as described below. The algorithms require a vector dataset as input, provided in a projected coordinate system that preserves distance measurements (e.g., UTM), representing individual polygon features of interest. It is not within the scope of this paper to describe mapping methods in great detail; instead it is assumed that features of interest have already been mapped, such as through manual mapping and interpretation of aerial/satellite imagery (e.g., Google Earth), automated classification that results in vectorized polygons based on geometric and radiometric image content (e.g.,

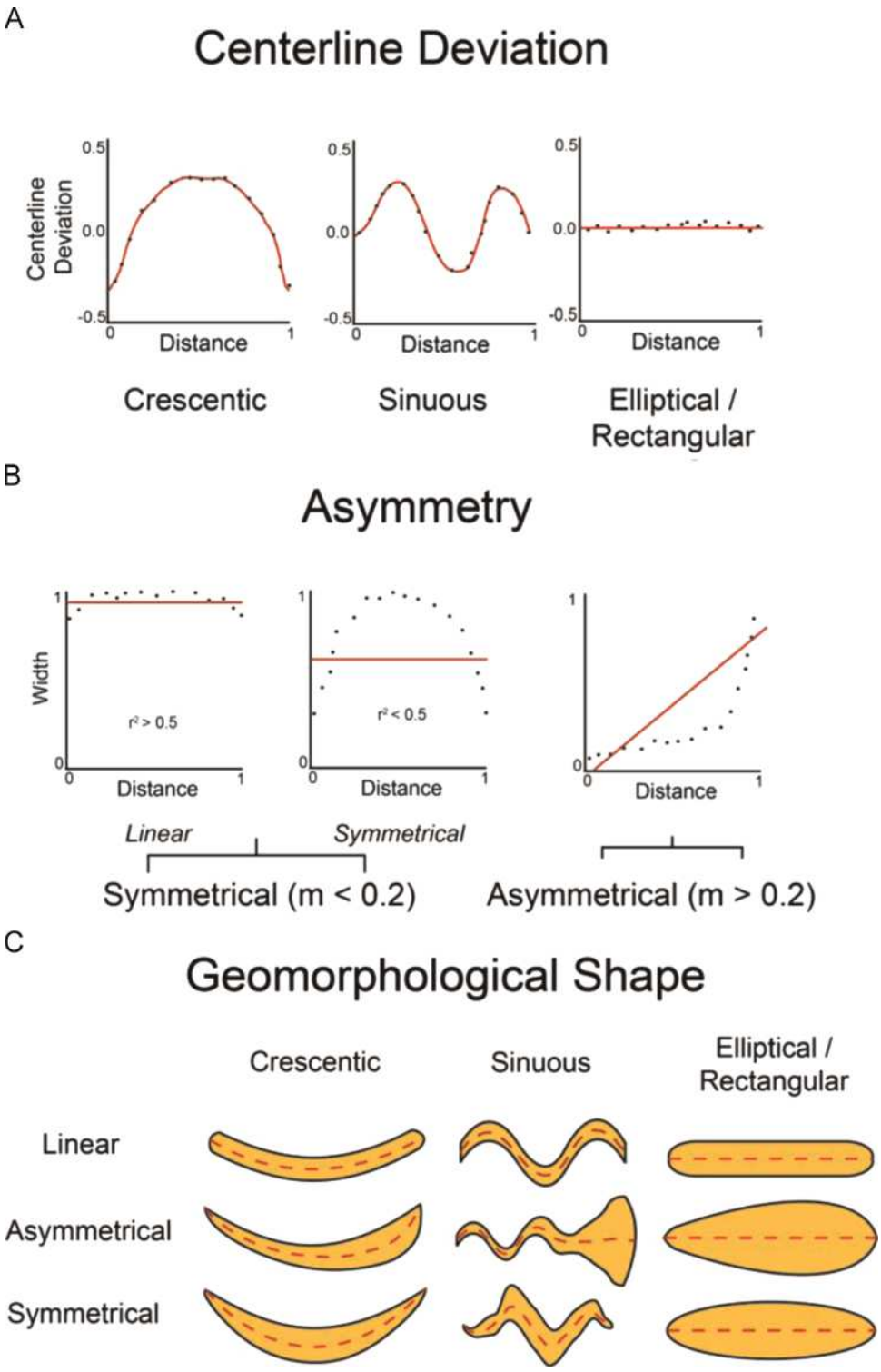

Fig. 6. (A) Centerline deviation with a normalized graph along distance, whereby a value close to zero indicates no deviation; (B) asymmetry, whereby a combination of slope and linear regression coefficients determine whether an object is linear, symmetrical or asymmetrical. (C) The geomorphological shape of a feature can be determined by combining centerline deviation (A) and asymmetry (B).

Maximum Likelihood), or a combination of the two. The proposed algorithms are described below.

2.1. Centerline

The centerline of an object is used to define the length of an individual shape within its spatial context. Numerous solutions have been proposed to define that centerline, particularly within the fields of computer science, mathematics and the medical sciences (McAllister and Snoeyink, 2000; Bouix et al., 2005; Cornea et al., 2007; Haunert and Sester, 2008; van der Werff and van der Meer, 2008; Lakshmi and Punithavalli, 2009; Wang et al., 2011). The most common solution is to define a skeletal line representation of each individual feature using Voronoi tessellation lines that calculate line segments as the furthest from all input vertices defining a particular polygon (Fig. 1A). The Voronoi

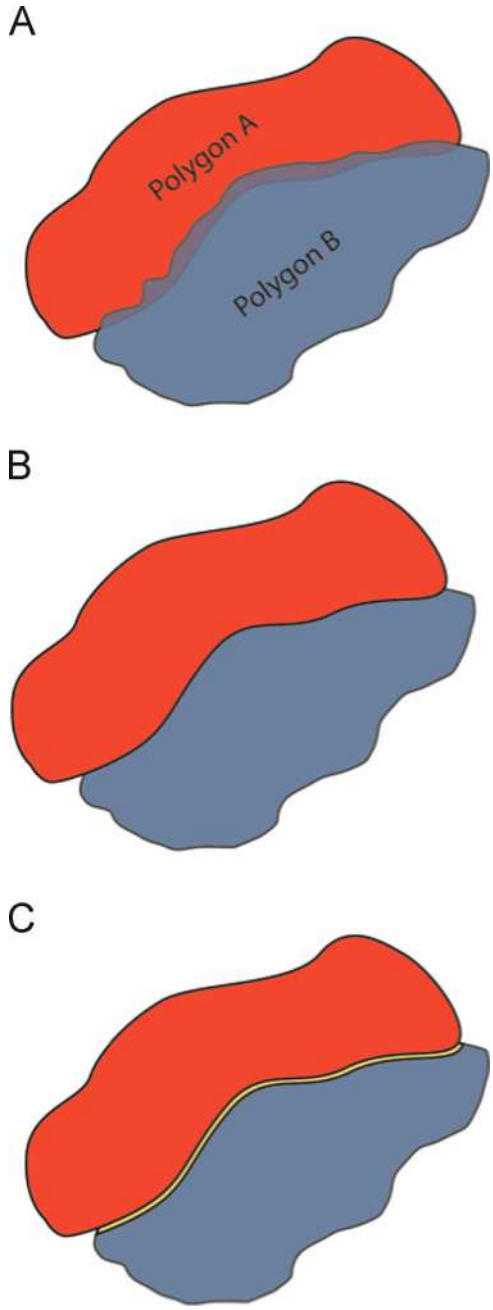

Fig. 7. Schematic showing workflow for calculation of the shared perimeter between two objects, Polygon A and Polygon B. (A) Overlap of two mapped features; (B) border corrected so that the perimeter is shared; (C) buffers each object by a given amount to create a new sliver polygon with the shared border length taken as half the perimeter of this.

(Thiessen) algorithm was selected here, as it is a standardized procedure available in most GIS suites, although any skeletal line generation is appropriate.

Typically the centerline of an individual polygon is generated by "pruning" the skeletal lines (Svensson and Sanniti di Baja, 2003; Bouix et al., 2005; Palágyi et al., 2006), by continuously removing peripheral lines at the polygon boundary until only the line segments in the center remain. However the complexity of modern depositional elements make it difficult to apply this in reality without losing information, as the amount required to be pruned varies according to geometry, shape and size (Fig. 1B). Rather, the centerline recovered here defines the longest cumulative or multiple line segment distance between one-to-one (Fig. 1B) or one-to-many end vertices (Fig. 1C) within a skeletal line graph (Hagberg et al., 2008).

Fig. 2A illustrates a simple centerline between two end vertices (start and end), which describes the centerline as the shortest distance between these two endpoints. The two endpoints are selected automatically using a double single-source Dijkstra algorithm (Dijkstra, 1956) to select a random seed within the skeletal line graph to determine the start coordinates as those which are furthest away from the initial seed. A second cumulative distance from this start point selects the end point and defines the centerline of the feature as well as the set of vertices that comprise the shortest path between the selected vertices. Removing all peripheral lines at the polygon boundary within a skeletal line graph until only line segments in the center remain, combined with a simple centerline as defined previously (Fig. 2A), will describe all potential paths between start and end vertices (Fig. 2B). Furthermore, the approach can be expanded to centerlines with multiple endpoints by treating each branch as its own individual shape.

One assumption for a centerline with multiple endpoints is that it will have a clearly defined branch that deviates from the main centerline, depending on a subjective interpretation of the threshold used to constitute a branch (Figs. 1C and 2C). This can be calculated by pruning the skeletal line until the minimum desired number of segments (a function of length) of a branch is reached. The Dijkstra algorithm calculated from each endpoint of the individual branches determines the furthest cumulative distance, ensuring that it does not double back on itself. This allows for identification of each branch while retaining the full length, rather than a pruned subsample. In essence, each branch along the centerline is treated as a single centerline feature. In a morphological context, this is particularly useful in defining the trend of channel width downstream in a distributive fluvial system (e.g.,Weissmann et al., 2010).

2.2. Centerline orientation

The automatically-generated centerlines are obtained without consideration of depositional dip direction (i.e. the start and endpoints are randomly defined according to the seed used to initiate the centerline calculation). This would result in undesirable consequences when orientation and width along the centerline is measured in relation to distance along a channel or other depositional element. In order to properly model the direction of the centerline, the relationship between the depositional system orientation and the centerlines of the modeled polygons must be established. This is achieved by using a semi-automated method that takes a manual interpretation of the land-/basinward direction of the depositional system and assigns the start vertex of all centerlines as the coordinate that is closest to the manually interpreted referenced line (Fig. 3).

By measuring the distance along a depositional system (Fig. 3A), the start coordinate of each individual feature is defined as the shortest cumulative distance along the reference line. This function corrects the orientation of the centerline of a feature and measures the distance along the fluvial system to each individual feature (see Congo River case study below). In marine settings, the start of beach and chenier ridge centerlines can be defined to start in relation to the closest distance to a channel (Fig. 3B). Once an appropriate centerline has been obtained for the desired polygon, the orientation is determined using the endpoint coordinates of the shortest path by $a \tan\left(\frac{\Delta y}{\Delta x}\right)$, relative to grid north. The shortest path is defined here as the distance between the start and end coordinates of the centerline. The orientation serves as an important component in determining change in geometric attributes

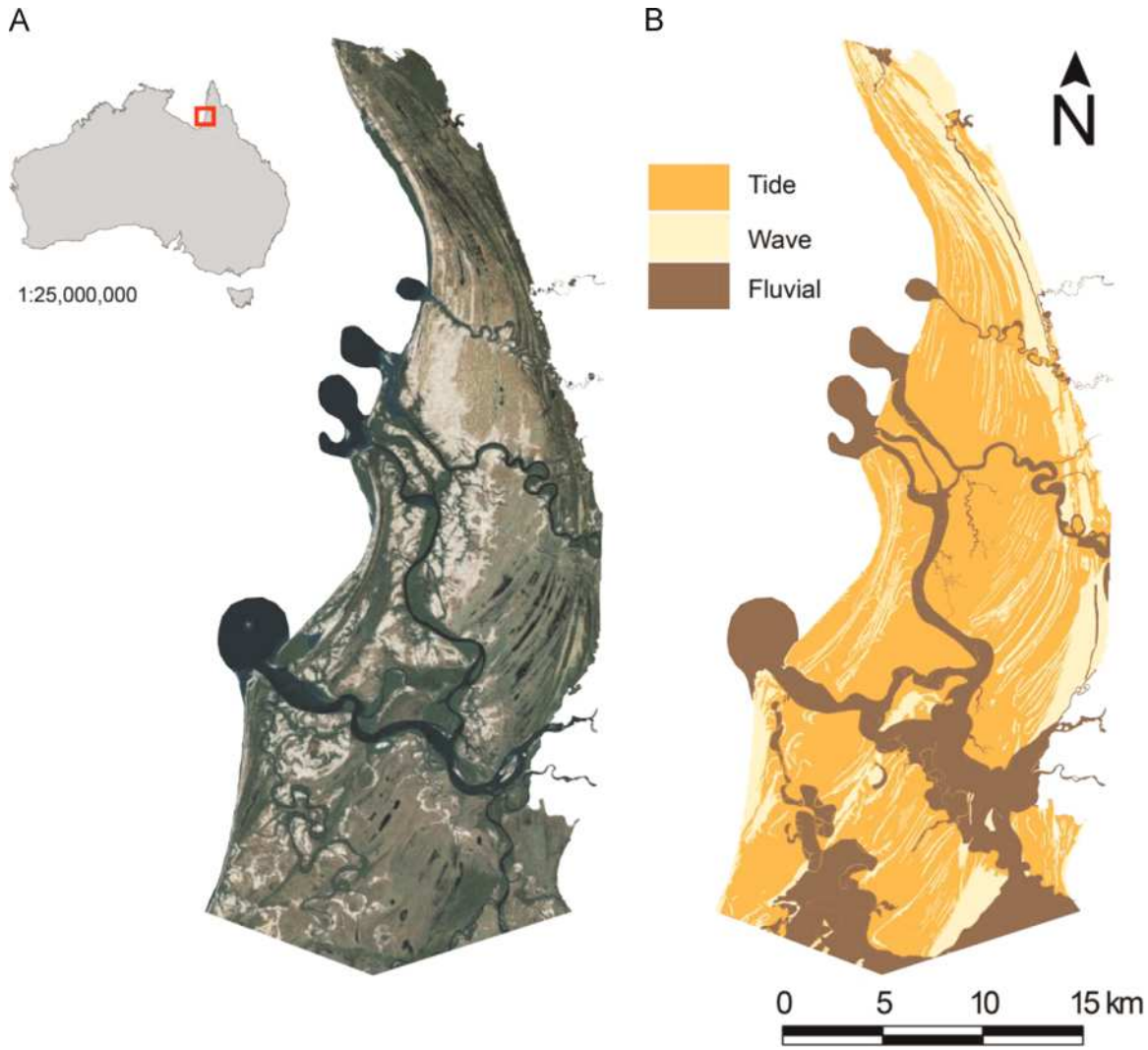

Fig. 8. (A) The Mitchell River Delta; (B) dominant processes of each depositional element (from Nanson et al., 2012). Background imagery© Bing™. Tide elements dominate the spatial extent of the delta, though potential reservoir elements are comprised of the less extensive fluvial and wave elements.

Table 1
The % of the total perimeter within each category of beach ridges, chenier ridges, channels or channel bars that are connected to one of the six major reservoir or non-reservoir elements in the Mitchell Delta dataset. Reservoir elements comprise beach ridges, chenier ridges, channels and channel bars (including mouthbars). The two main non-reservoir elements of swales, and tidal flats and floodplains demonstrates the dominate heterogeneity associated with each reservoir element. See Nanson et al., 2012 for a complete discussion on depositional elements.

		Reservoir				Non-reservoir			
		Beach Ridges	Chenier Ridges	Channels	Channel Bars	Swales	Floodplains / Tidalflats	Other	Total
Reservoir	Beach Ridges	32.6	0.4	0.6	0.5	46.1	17.0	2.9	100.0
	Chenier Ridges	0.5	12.8	0.2	0.3	26.7	57.4	2.0	100.0
	Channels	2.6	0.7	1.9	52.2	1.9	32.1	8.6	100.0
	Channel Bars	1.6	0.7	37.1	11.6	0.0	18.1	30.9	100.0

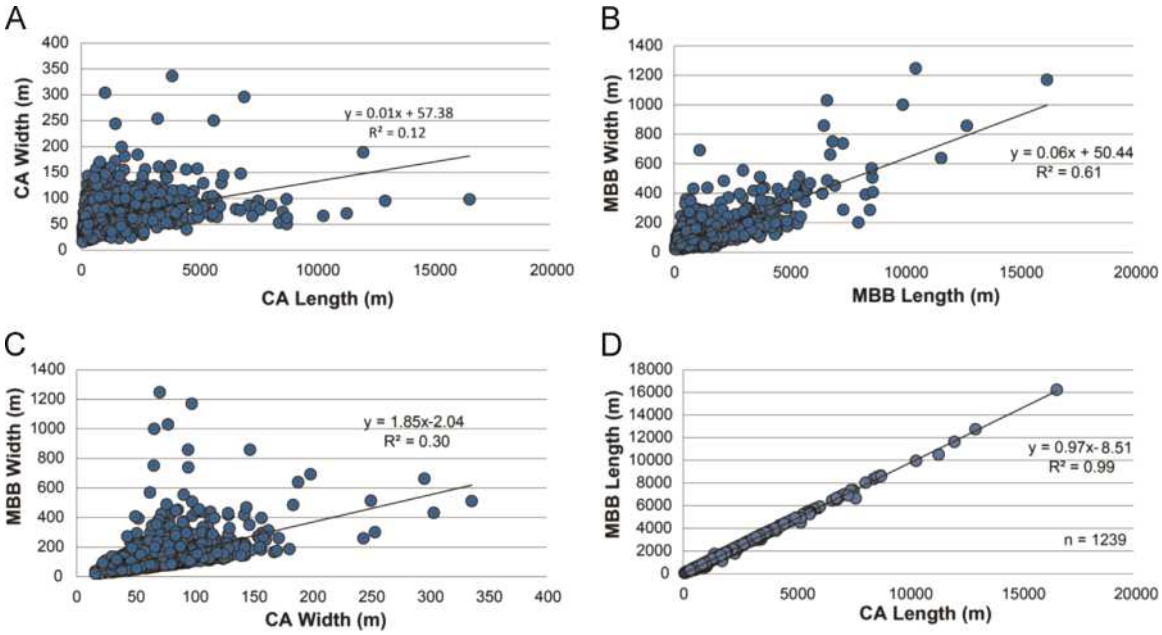

Fig. 9. (A) wave-generated elements (beach and chenier ridges) CA width to length shows a weak correlation, suggesting that the width of wave-generated elements do not increase with length. (B) MBB width to MBB length reproduced after the method of Nanson et al. (2012). (C) MBB width to CA width overestimates MBB width, when (D) MBB length to CA length shows that the length is only slightly underestimated. The greatest source of error is associated with the width measurement from the MBB method.

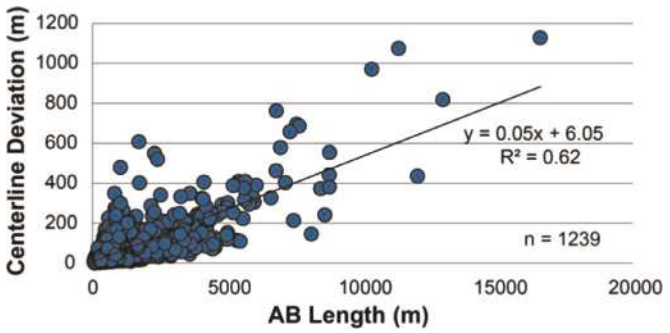

Fig. 10. CA length versus centerline deviation for wave-generated elements shows a strong correlation, with a similar linear regression line to that of the MBB length versus MBB width plot in Fig. 9B. This shows that a MBB measurement of the crescentic wave-generated elements of the Mitchell Delta captures the crescentic shape of elements rather than its width.

within a depositional environment of interest.

2.3. Centerline deviation

The ratio of the centerline length over the shortest path length yields a feature's sinuosity; however, sinuosity is of limited value as it is only a single measurement taken over the entire length of the element, and does not consider its variation over distance. For example, multiple sinuosity measurements may be more appropriate to describe larger features, such as rivers, though the granularity must be carefully chosen to be representative of the actual sinuosity in subdivided regions. This is an issue when in quantitative analysis of elements that vary significantly in centerline profile and length.

We propose to calculate centerline deviation using the perpendicular distance from the shortest path to the centerline (Fig. 4), calculated at a user-defined sample spacing. This deviation, calculated along the centerline, can be used to establish parameters such as amplitude and variability as a function of distance. The advantage over a conventional sinuosity measurement is that features with similar sinuosities but different geomorphological characteristics can be differentiated.

2.4. Width

For each centerline deviation, a corresponding width measurement is taken perpendicular to the centerline and bounded by the polygon's spatial extent. This measurement is taken perpendicular to the angle between the endpoints of twice the user specified distance with the measurement being placed at the end of the first line (Fig. 5). Considering that the midpoint of the perpendicular line is created at the endpoint of the first line segment, a measurement of distance versus width can be determined. The width is calculated from the points where the perpendicular line intersects the boundary of the original feature on either side of the centerline, resulting in a line that contains three vertices: the midpoint and the two intersection points on the boundary.

The reliability of automated width measurements depends on two main criteria: the closeness of the centerline representation to the true element centerline, and the sampling distance chosen for each calculated measurement. As the perpendicular line is taken in relation to the centerline, a poor centerline representation may yield an unreliable width measurement (Fig. 5B). The fidelity of the centerline depends principally on the vertex sampling of the enclosing polygon, which is defined in the centerline creation process, and is itself based on the input vector mapping data. Low sampling frequency may result in an unrepresentative width measurement, as the perpendicular line is taken at a spacing lower than the variability present in the dataset (Fig. 5C). Taking a higher density of measurements at a shorter interval may solve the issue; however, the sampling must be chosen to be adaptive to elements from modern deposition systems of variable size. Therefore, to reduce the computational complexity whilst retaining equal sample spacing, an optional implementation is suggested to only take the n^{th} sample per shape. Although an adaptive sampling would be beneficial to ensure appropriate point spacing in both straight and curved sections, in this case equal spacing is preferred to define geometric shape in the geomorphological classification (Section 2.5).

After automated width extraction there will undoubtedly be misrepresentative measurements, owing to the inherent complexity found in nature, and which need to be removed or

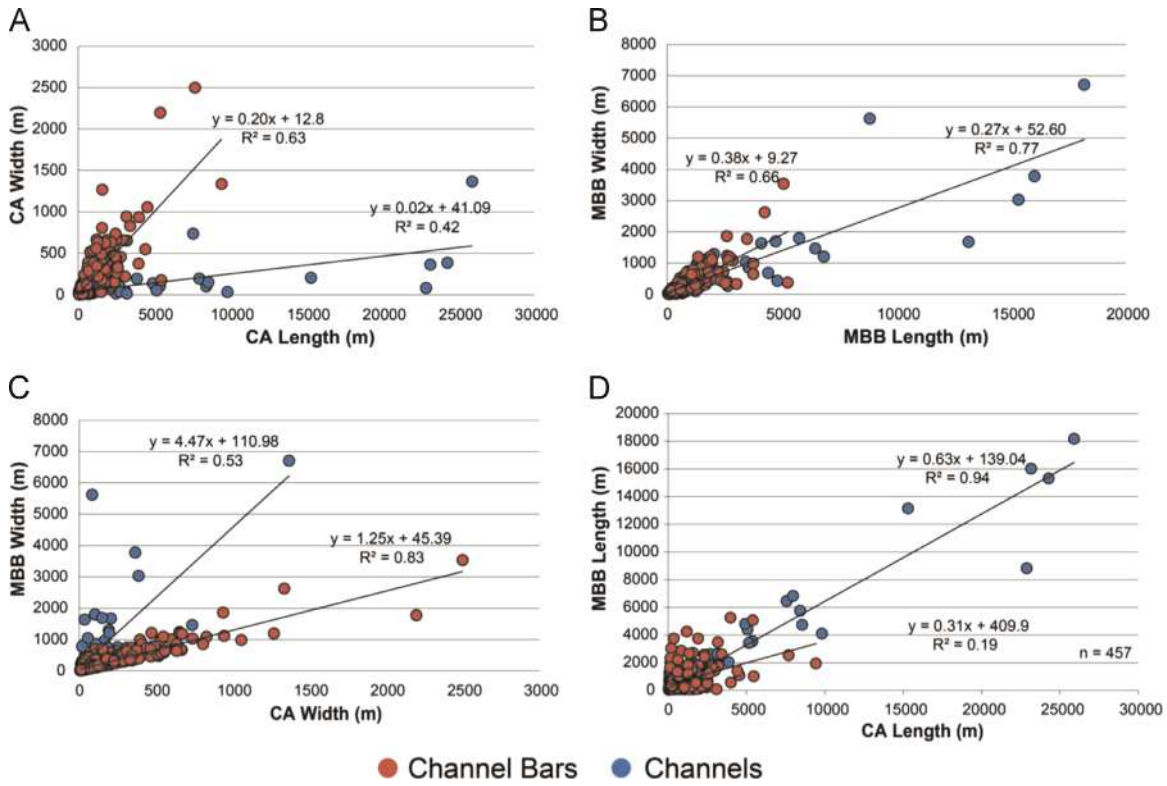

Fig. 11. (A) Compares fluvial generated elements (channels and channel bars) CA width to length and MBB width and MBB length in (B). A comparison of MBB width to CA width is shown in (C) and a MBB length to CA length in (D). These results suggest that MBB overestimates the width of features while underestimating length implying any MBB relationship of length versus width may be unreliable.

corrected. The true width of any given feature is defined by the perpendicular lines on each side of the centerline being exactly equal (Fig. 5D). By providing a threshold factor that determines the maximum allowed percentage difference between each side, lower quality width calculations can be removed. Alternatively, those width measurements flagged as low quality can be interpolated from the surrounding width measurements using, for example, a polynomial function.

2.5. Geometric shape

Once length, centerline deviation and width have been defined along the centerline at the specified sample spacing, these geometric attributes can be used to make an objective classification of geomorphological shape. An object is described as belonging to one of nine classes through a combination of crescentic, sinuous or ellipse/rectangular shapes (Fig. 6A), with linear, symmetrical or asymmetrical characteristics (Fig. 6B) which combine to indicate geomorphological shapes (Fig. 6C). To describe these geometric shapes, four parameters (sinuosity, crescentiformity, symmetry and linearity) are combined to segregate the classes mentioned.

The sinuosity threshold determines whether an object is crescentic/sinuous or ellipse/rectangular, as defined by the ratio of the maximum deviated centerline divided by half the maximum width. A value below one indicates that the shortest path of the centerline is contained completely within the modeled object, while a value approaching zero (i.e. no sinuosity) suggests either an ellipse or rectangular feature (Fig. 4A). In contrast, a value greater than one would indicate a feature whose amplitude is greater than width, indicating extreme sinuosity or potentially a crescent-like shape. By examining the proportion that the centerline deviates to one side or the other from its shortest path, a crescentic threshold, defined as greater than 80% on one side, determines that the object is crescentic rather than sinuous (Fig. 4B).

Each classification of sinuous, crescentic or elliptical/rectangular shape on the *X*-axis (Figs. 4A, and 6A) is combined with its linear, symmetrical or asymmetrical geometric planform on the *Y*-axis (Fig. 6B). This planform is based on a symmetry threshold which defines whether a feature is symmetrical or asymmetrical in terms of an equal distribution of width to distance. For any given feature on a linear regression slope, if the width versus distance is greater than an empirically-defined symmetry threshold of 0.2, then that characteristic feature is classified as asymmetrical. Finally, if the feature is not asymmetrical, the linearity threshold examines the coefficient of determination (r^2) of a linear regression line for each individual object, classifying an object as linear when r^2 is greater than 0.5. Otherwise a feature is assigned as symmetrical (Fig. 6B).

2.6. Adjacency

The heterogeneity between depositional elements, and subsequent adjacency seen in a depositional system, play an important factor in determining the relationship between elements, providing an understanding of the potential fluid flow dynamics in the subsurface (Howell et al., 2008). The variance in adjacency of depositional elements in different modern depositional systems provides a relative and quantitative measurement to compare the degree and proportion of heterogeneity that may be preserved. The adjacency of depositional elements can be measured in several ways, and two possibilities are considered here: (i) the instances of features sharing a single edge, representing the number of neighboring sandbodies and the number and distribution of elements; (ii) the surface area (perimeter) that spatially connects these elements in the depositional system.

To examine the instances where a polygon shares at least a single edge with another feature can be achieved by calculating

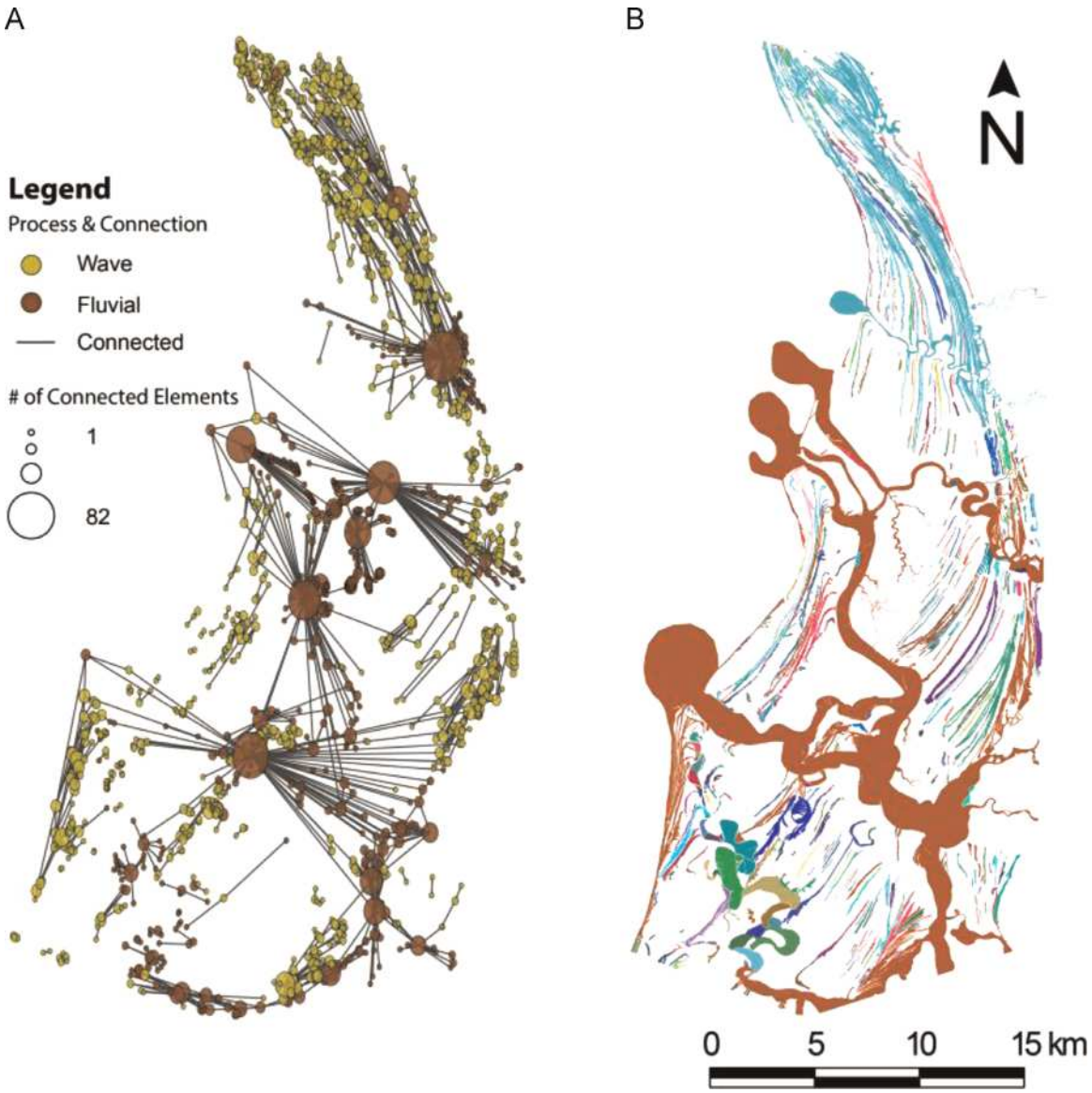

Fig. 12. (A) Represents wave and fluvial element locations by their centroid coordinates, with node sizes relative to the number of reservoir elements it connects. (B) shows a random color coded scheme based on the 498 connected individual sandbody groups. The original geometry and attributes of individual elements within each group is retained by grouping the reservoir elements by their connection in A rather than merging and dissolving their adjacent boundary (see Fig. 5 in Nanson et al., 2012). (For interpretation of the references to color in this figure legend, the reader is referred to the web version of this article.)

any overlap or intersection between their vertices and registering that by a unique identifier. This groups all adjacent shapes while retaining their original shape and attributes, without the need to merge the complex shapes that would otherwise remove any additional attributes of each component polygon.

To examine the shared perimeter between two or more polygons is more complex, and is dependent on the given input vector data, as adjacency will be disturbed when shared edges do not have equal vertices. To ensure that the shared part of a polygon's border is identical in all surrounding polygons, any given overlap is removed to create a new set of features, the geometry of which is revised (Fig. 7A and B). If small gaps are present between the revised polygons, a buffer can be assigned to the operation above to ensure that overlap will be present. Despite a cleaned input vector dataset, the vertices that comprise the shared border may still differ, rendering a perimeter calculation between all polygons invalid. One solution to this challenge is achieved by buffering each polygon by a proportion of its relative scale, and the perimeter of the resulting sliver polygon is halved to give the shared border length (Fig. 7C).

3. Case studies

To show the applicability of the described geometric attribute descriptions two different depositional environments are described, which represent a variety of scenarios that may improve geometric analytical capability. These include a comparison of geometric attributes and spatial connectivity from the Mitchell Delta, Gulf of Carpentaria, Australia – a tropical, tide-dominated, fluvial-influenced, and wave-affected marginal marine system (Nanson et al., 2013). Secondly, the method was a applied to the tropical intracratonic fluvial system of the Congo River, Democratic Republic of the Congo (Kadima et al., 2011), to assess attribute change analysis over 1200 km of the river's extent.

The minimum bounding box's shortest axis (width) and longest axis (length), hereby referred to as a MBB width and MBB length, have been used in a geomorphological context in a wide range of

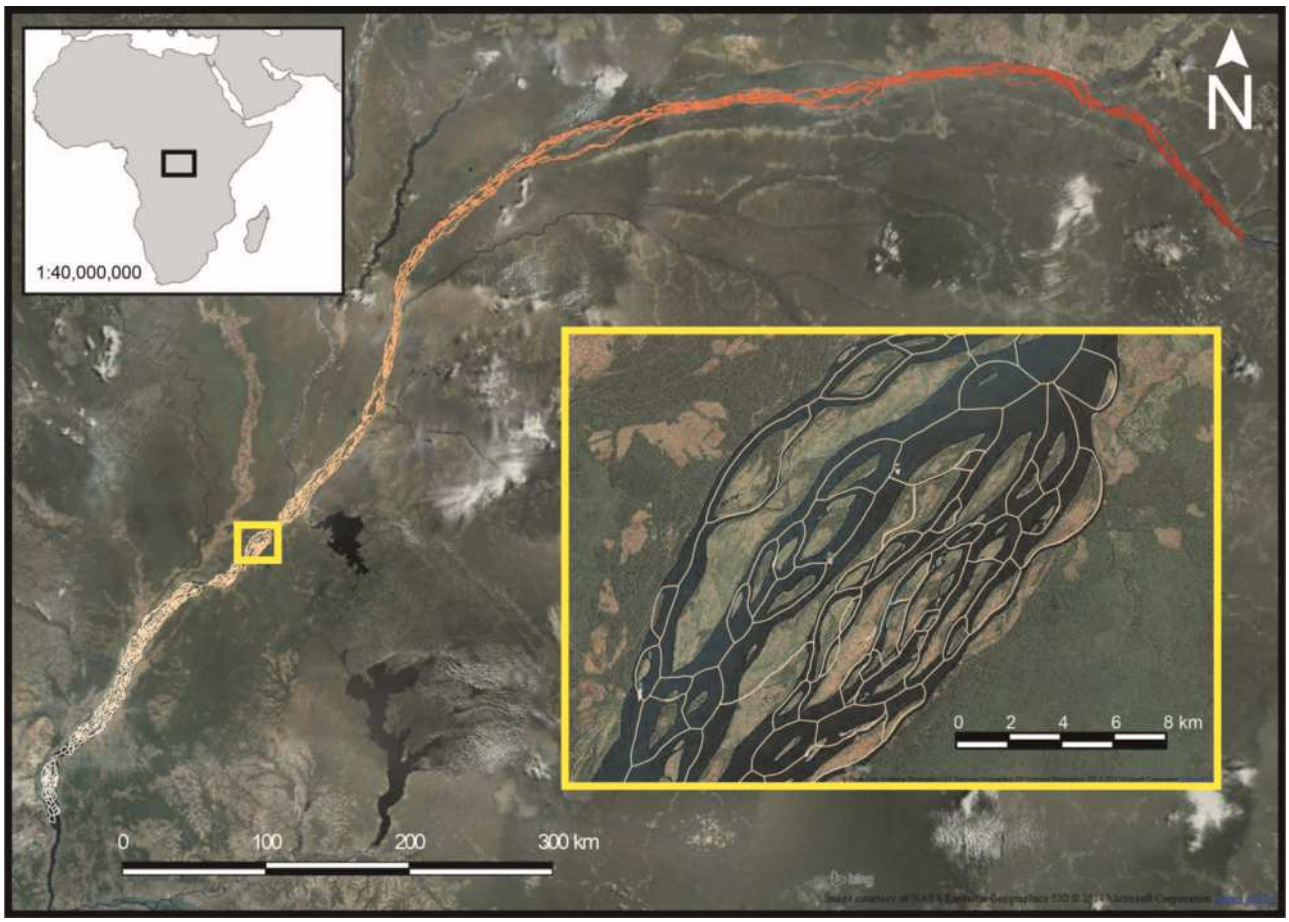

Fig. 13. The Congo River dataset showing the centerlines of the anabranching river with a colored increase indicating the cumulative distance upstream from 0 to ~1200 km. A zoomed subsection is shown that also represents the subsection used to illustrate the centerline correction, width and centerline deviation analyses performed on the mid-channel bars in Fig. 14. Background imagery© Bing™.

fields (e.g., Gardoll et al., 2000; Côté and Burn, 2002; Shugar and Clague, 2011; Nanson et al., 2012) to facilitate the automated quantitative geometric attribute and shape characterization. The case studies below also use a MBB algorithm by width for a direct comparison of geometric attributes to the proposed CA methodology.

3.1. Mitchell Delta

The 520 km^2 northern Mitchell River Delta dataset consists of 1696 potentially preserved reservoir elements (mouthbars, channel bars, channels, abandoned channels, cheniers and beach ridges), mapped using a combination of high resolution satellite imagery, ground truthing, augering, digital elevation model (DEM) analysis, trenching and surface sampling (Nanson et al., 2012). Elements were analyzed using the CA method, with centerline deviation and width measurements taken every 50 m up to a maximum sampling number of 100 and to an accuracy of 10%.

Using the CA methodology, the geomorphological shapes of potential reservoir elements in the Mitchell Delta show a wide distribution, similar to the findings of Nanson et al. (2012) who used a manual approach. The elements are predominantly elliptical and crescentic in form, excluding the meandering channels. Beach and chenier ridges are mostly asymmetrical ellipses (30% and 23%) and asymmetrical crescents (29% and 30%), mouthbars and pointbars are symmetrical crescents (75%, and 24%) and asymmetrical crescents (25% and 47%), whilst midbars are mainly asymmetrical ellipses (61%).

The results from the CA method suggest no discernable trends of width with length (Fig. 9A) for wave generated processes (beach ridges and cheniers). This shows a relatively constant mean around 65 m ($\pm$ 32 m). In contrast, the results of MBB width versus MBB length show a trend that can be represented by a linear regression line (Fig. 9B). Indeed, a comparison of the two methods show that MBB overestimates CA width by a linear regression at 1.85x (Fig. 9C) and underestimates CA length at 0.97x (Fig. 9D). One explanation for this difference is demonstrated by a measurement of maximum centerline deviation versus length indicating a strikingly similar trend to MBB width and MBB length comparison (Figs. 9B and 10). Datasets with predominantly crescentic shapes greatly exaggerate the MBB width given the long features that are present, a fact emphasized by the maximum width values present in a MBB compared to a CA width measurement.

The geometric attributes from fluvial reservoir elements, split into channels and bars, indicate a similar disparity. While the CA method (Fig. 11A) and the MBB method (Fig. 11B) both show a trend of width versus length, the range of values is different where MBB overestimates widths (Fig. 11C) and underestimates lengths (Fig. 11D). For example, channel bars show a regression slope of the MBB measurements at nearly twice that of a CA measurement (0.38 versus 0.20). The mean MBB width-to-length ratio is 0.42, falling outside the typical range between 0.15 and 0.35 by previous manual measurements of mid-channel bar forms (Holzweber et al., 2014), compared to 0.24 in this study.

Fig. 12A shows an illustration of all the shared borders between reservoir elements in the Mitchell Delta (see Fig. 8). These connections are achieved mostly through a shared border with fluvial

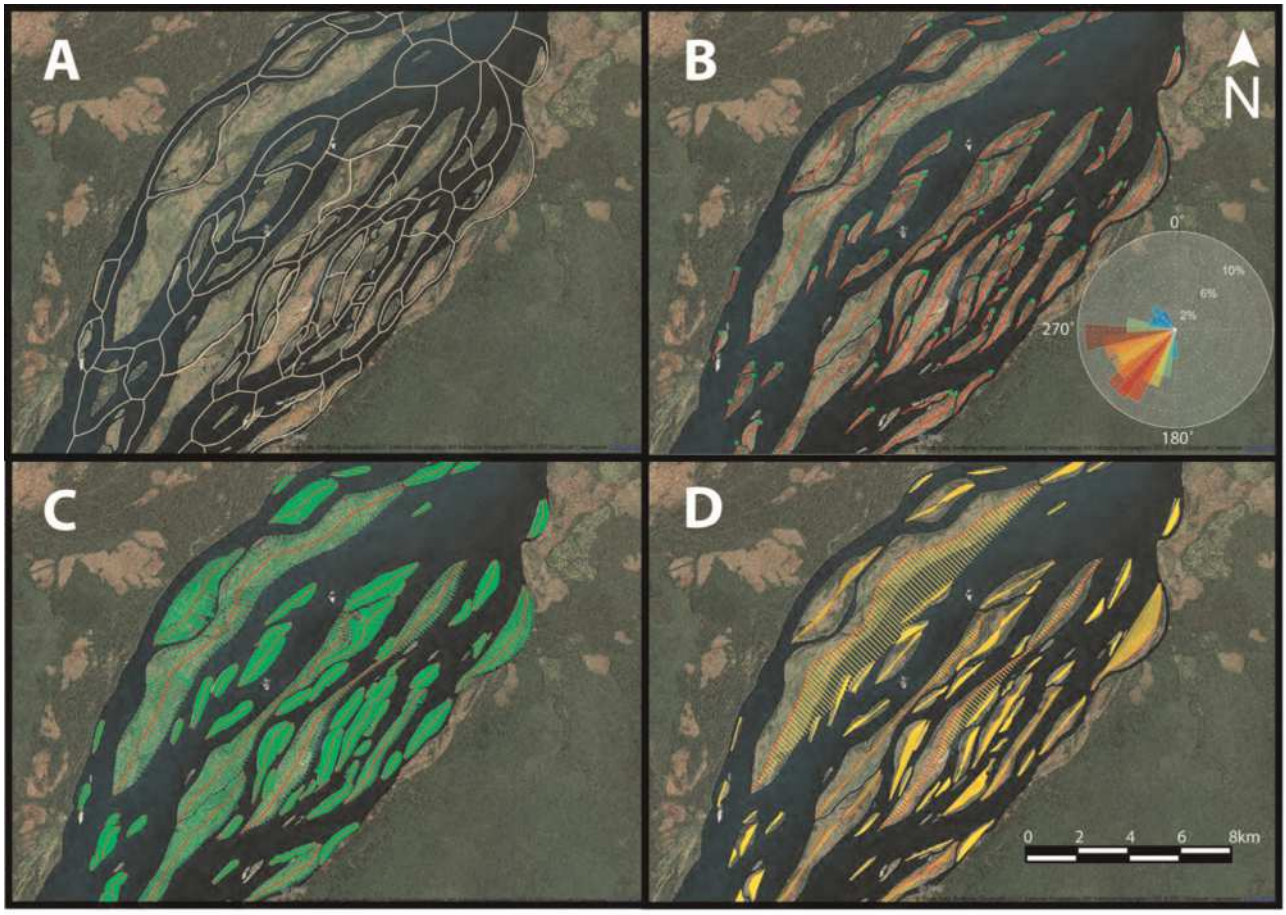

Fig. 14. A subsection of the Congo, see box in Fig. 13, used to show the original image in (A), and centerline generation in (B) with its start vertex corrected upstream along the river. A rose diagram is used to show the direction of all mid-channel bars in Congo River. This centerline can subsequently be utilized to generated equally spaced width measurements in (C) and centerline deviation in (D). Background imagery© Bing™.

elements (i.e. channels), with up to 82 neighboring connections. The majority of single sandbody compartments are isolated chenier ridges and a small proportion of beach ridges. The 2D adjacency of the Mitchell Delta (Fig. 12B) is represented by 498 individual connected sandbodies, where the two largest connected sandbodies comprise 592 and 320 individual features ($>50\%$ of total) and an area of 125 km^2 ($>70\%$ of total). The largest connected sandbody by area consists of predominantly fluvial features (82%), whereas the second largest set of connected sandbodies is mainly wave-generated (79%).

While these results suggest that fluvial elements provide a significant degree of adjacency (Fig. 12A and B), the shared border between fluvial and wave-generated elements is minimal (Table 1). For channels, the highest connected element type are channel bars (52.2%) and non-reservoir element of tidal flats and floodplains (32.1%). Conversely, channel bars are predominantly connected to those channels whereas midbars are enclosed by the channel and channel sidebars having at least a 50% non-reservoir connection. Channel-to-beach and channel-to-chenier ridge connections show low levels of adjacency (2.6% and 0.7% respectively). Beach and chenier ridges show a high degree of inter-adjacency, with beach-to-beach ridge connections reaching 32.6% and chenier-to-chenier connections at 12.8%, suggesting clustering. The main heterogeneity with beach ridges are swales (46.1%) and tidal floodplains (17.0%), compared to tidal floodplains (57.4%) and swales (26.7%) for chenier ridges.

3.2. Congo River

The Congo River basin data is derived from Landsat 7 Enhanced Thematic Mapper Plus (ETM+) imagery available from the Landsat Global Land Survey 2000 dataset (USGS, 2009) and accessed through the seamless global coverage available within the Landsat-ESRI collaboration (ESRI, 2014). This imagery has a spatial resolution of 30 m in 6 spectral bands, as well as one 15 m panchromatic band and one 60 m thermal infrared band. The multispectral data were processed in ArcGIS™, using a supervised classification to highlight the spectra of water in the dataset to identify the main river channel (Fig. 13). The internal structures within the anabranching river were assumed to be the mid-channel bars (Fig. 14).

The Congo River dataset extends 1200 km, with an average width of 8.2 km and contains 2221 mid-channel bars. The centerline orientations of the mid-channel bars were corrected according to the distance along anabranching river centerlines, with start vertices assigned upstream along the Congo River (Section 2.2; Fig. 14A and B). Width measurements of the anabranching river were calculated every kilometer, with an accuracy of 1%. The width and centerline deviation of the mid-channel bars (Fig. 14C and D) were taken every 25 m at a maximum sampling interval of 100 and to an accuracy of 10%.

The results show that the geometric shape of the mid-channel bars in the Congo River basin are split into ellipse (92%), crescentic (7%) and sinuous (1%) shapes, with the majority being asymmetrical (71%) as opposed to symmetrical (28%) and linear (1%) planforms. Ninety percent of the asymmetry within the Congo

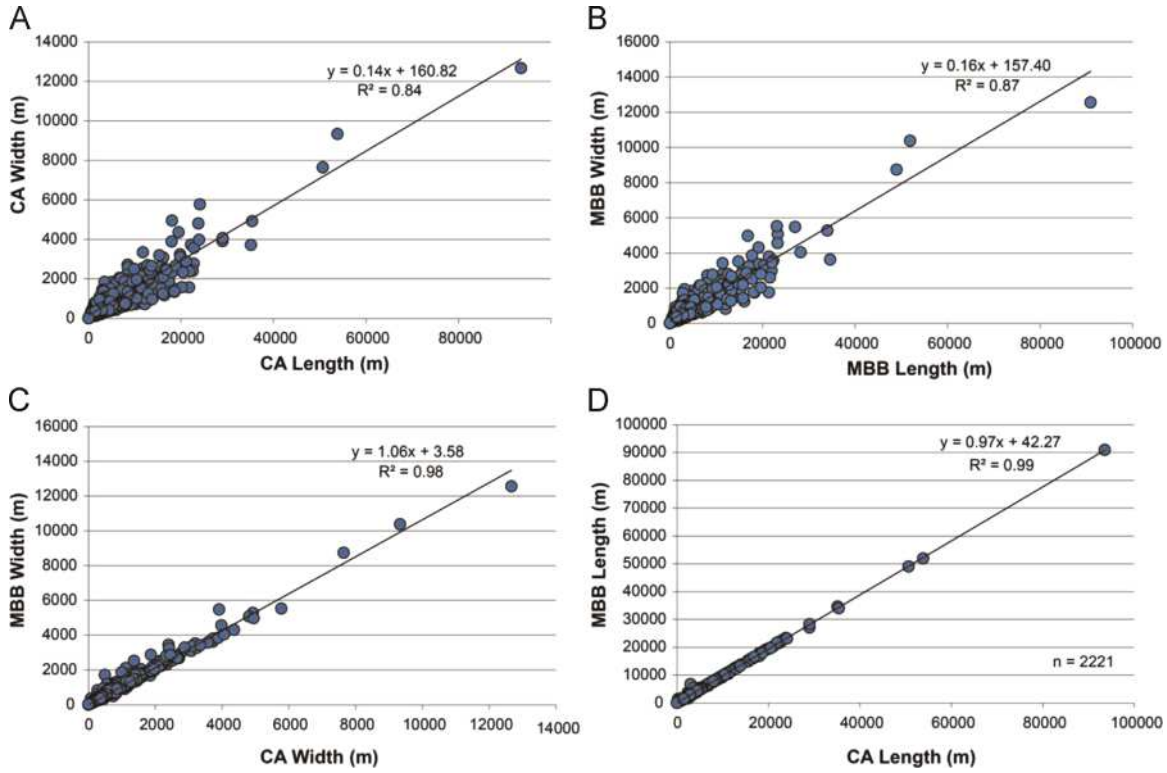

Fig. 15. (A) Compares CA width to length features of mid-channel bars in the Congo River. (B) Shows MBB width and MBB length of those same bar forms. A MBB width to CA width comparison is shown in (C) while (D) shows a MBB length to CA length comparison. The strong correlation between the CA and MBB suggests that both methods produce reasonable measurements for the predominately ellipse shapes of the mid-channel bars of the Congo River.

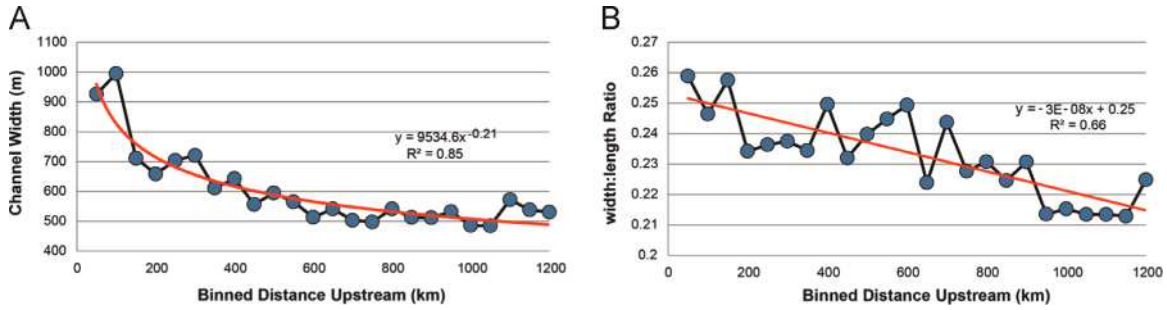

Fig. 16. Average channel width and width:length ratio binned into 50 km sections along the Congo River showing that both channel width (A) and width:length ratio (B) decrease with distance upstream.

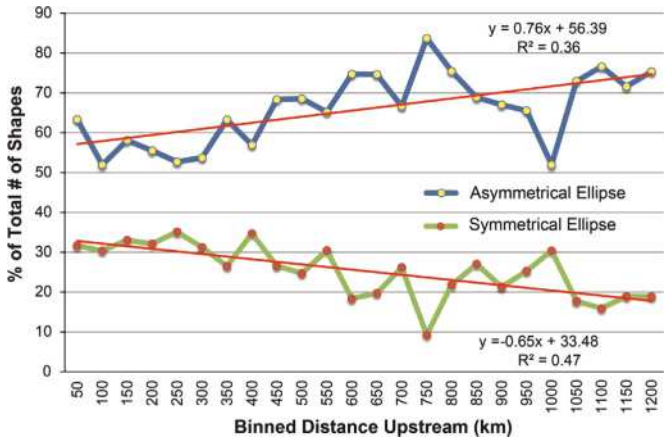

Fig. 17. Change in proportion of asymmetrical and symmetrical ellipses as a % of total with distance upstream along the Congo River binned into 50 km sections.

River basin is oriented upstream. The width-to-length ratio of all mid-channel bars demonstrates a strong relationship, with an arithmetic mean of approximately 0.16 (Fig. 15A). The regression slopes for the MBB width and MBB length method for mid-channel bars in the Congo River (Fig. 15B) are very similar to those proposed in this paper, 0.16 versus 0.14, respectively. Specifically, a comparison of width measurements (Fig. 15C) shows a slight overestimation of MBB geometry with a regression line at 1.06*x* and a slight underestimation of MBB length at 0.97*x* (Fig. 15D). The mean width-to-length ratio found by the CA method is 0.23, compared to 0.25 from the MBB approach.

Analysis of mid-channel bar width to length and channel width binned by distance upstream of the Congo River (Fig. 16) shows a decrease in both variables. The mean width to length ratio of mid-channel bars downstream is 0.26, compared to 0.21 upstream. Channel width changes from a mean of 925–530 m. The change in geomorphological shape between asymmetrical and symmetrical ellipse mid-channel bars (the two highest represented proportions of the mid-bars in the Congo) shows an increase in asymmetry of mid-channel bars upstream (Fig. 17).

4. Discussion

The application of MBB to describe shape and geometry of geospatial data has been applied in the past due to its ease of use and accessibility within standard GIS suites. The width, length and area from a MBB provide the ability to measure maximum and minimum geometric values and the basis to describe shape, such as elongation and circularity (e.g., Gardoll et al., 2000; van der Werff and van der Meer, 2008; Tafesse et al., 2012; Kröner and Doménech Carbó, 2013). However the measurements derived from a MBB analysis are limited and our proposed method shows potential in describing the complexity of geometric shapes and element adjacency of modern depositional systems. The complexity of shapes and their geometries in subsurface reservoir models are important to quantify heterogeneities and compartmentalization (Larue and Legarre, 2004), and studies of modern systems can aid in differentiating planform geometries that vary by depositional environments (Tye, 2004; Nanson et al., 2012; Massey et al., 2013; Vakarelov and Ainsworth, 2013). The tools presented in this paper demonstrate progress towards achieving that goal in a quantitative and objective scheme.

The case studies have shown that in comparison to the conventional MBB approach, the present study has significant advantages for measuring the quantitative internal dimensions of target elements. The MBB method inherently exaggerates the width and underestimates the length of the polygon it is used to describe. As such, the use of these measures in describing the internal geometries of target elements provides potentially misleading results, as indicated by the Mitchell River Delta dataset. Conversely, the mid-channel bars of the Congo River were found to be well-represented by MBB geometry. This discrepancy is attributed to the greater complexity of elements found in the tide-influenced Mitchell Delta (Nanson et al., 2013), with more crescentic and sinuous shapes compared to the predominately elliptical shapes found in the Congo.

Adjacency between potential reservoir elements in the Mitchell Delta has been shown, with channels indicated as the most connected elements (Fig. 12A). While fluvial channels supply shorelines with the sediment needed to construct beach and chenier ridges (Rhodes, 1982), intervening non-reservoir elements can form barriers between fluvial and wave elements to reduce connectivity (Howell et al., 2008). This is significant, as of the channels and ridge forms that are connected, the connection pathways are often along narrow conduits of beach and chenier ridges (Table 1; Fig. 12B; Nanson et al., 2013) to considerably reduce the connectivity of the entire reservoir sandbody. If channels in the Mitchell Delta are mud filled after abandonment, this will further promote compartmentalization. A quantification of the connected sandbodies and the perimeter connecting sandbodies as proposed in the new methodology has allowed for another quantitative technique to compare the relative heterogeneity and compartmentalization between different modern systems.

In addition to the geometric attribute characterization, the proposed CA method has shown its broader applicability within geomorphology to study the variability in geometric attributes and shape with distance along a depositional system. As demonstrated by the Congo River study, this provides a unique insight into the change in shape classification and attributes for example, as channel width and symmetrical ellipse shapes decrease with distance upstream. This may reflect a transition from an open portion of the anabranching river to narrower channels and lower width: length mid-channel-bars upstream. Defining trends within depositional environments is an essential component in the framework of any depositional model (e.g., Boyd et al., 1992; Nichols and Fisher, 2007) and geometric attribute and shape characterization proposed in the methods here can help to quantify that variability using modern examples.

The case studies demonstrate the method using modern clastic depositional systems. However, there is a broader potential application to any two-dimensional object including carbonates (e.g., Harris, 2010). Another example within the geosciences is application to two-dimensional along strike or dip sections of outcrop analogues (e.g., Rittersbacher et al., 2013), where current methods to retrieve geometric attributes and describe element shape are largely performed manually and subjectively (Howell et al., 2014). Our method may address these limitations by adding automation and systematic measurement to reduce error.

5. Conclusion

This paper presents a method to calculate the geometric attributes in relation to shape and adjacency of mapped depositional features for improved empirical analysis in geomorphology. The method is implemented as a set of scripts for use in a GIS environment, where in-built capabilities have traditionally been lacking. By sampling multiple equally-spaced measurements of two-dimensional objects along their centerlines, a better representation of width and centerline deviation variability has been achieved compared to conventional GIS approaches. This systematic and objective measurement can be used to analyze the geomorphological shape of features and their distribution within modern depositional systems.

Acknowledgements

This work has been funded by the FORCE Sedimentology and Stratigraphy Group and the Norwegian Petroleum Directorate as part of Phase 2 of the SAFARI program. Two anonymous reviewers and the handling editor are thanked for their constructive input, which helped improve the manuscript.

Appendix A. Supplementary material

Supplementary data associated with this article can be found in the online version at http://dx.doi.org/10.1016/j.cageo.2015.06.003.

References

Benz, U.C., Hofmann, P., Willhauck, G., Lingenfelder, I., Heynen, M., 2004. Multi-resolution, object-oriented fuzzy analysis of remote sensing data for GIS-ready information. ISPRS J. Photogramm. Remote Sens. 58, 239–258.
Blaschke, T., 2010. Object based image analysis for remote sensing. ISPRS J. Photogramm. Remote Sens. 65, 2–16.
Bouix, S., Siddiqi, K., Tannenbaum, A., 2005. Flux driven automatic centerline extraction. Med. Image Anal. 9, 209–221.
Boyd, R., Dalrymple, R., Zaitlin, B.A., 1992. Classification of clastic coastal depositional environments. Sediment. Geol. 80, 139–150.
Cornea, N.D., Silver, D., Min, P., 2007. Curve-Skeleton Properties, Applications, and Algorithms. IEEE Trans. Vis. Comput. Graphics 13, 530–548.
Côté, M.M., Burn, C.R., 2002. The oriented lakes of Tuktoyaktuk Peninsula, Western Arctic Coast, Canada: a GIS-based analysis. Permafr. Periglac. Process. 13, 61–70.
Dijkstra, E.W., 1956. A note on two problems in connexion with graphs. Numerische Math. 1, 269–271.
ESRI (Environmental Systems Resource Institute), 2014. ArcMap 10.1. ESRI, Redlands, California.
Fisher, G.B., Bookhagen, B., Amos, C.B., 2013. Channel planform geometry and slopes from freely available high-spatial resolution imagery and DEM fusion: implications for channel width scalings, erosion proxies, and fluvial signatures in tectonically active landscapes. Geomorphology 194, 46–56.
Freeman, H., Shapira, R., 1975. Determining the minimum-area encasing rectangle for an arbitrary closed curve. Commun. ACM 18, 409–413.
Gardoll, S.J., Groves, D.I., Knox-Robinson, C.M., Yun, G.Y., Elliott, N., 2000. Developing the tools for geological shape analysis, with regional- to local-scale

examples from the Kalgoorlie Terrane of Western Australia. Aust. J. Earth Sci. 47, 943–953.
GRASS Development Team, 2014. Geographic Resources Analysis Support System (GRASS) Software. Open Source Geospatial Foundation Project.
Hagberg, A., Schult, D., Swart, P., 2008. Exploring network structure, dynamics and function using NetworkX. In: Varoquaux, G., Vaught, T., Millman, J. (Eds.), Proceedings of the 7th Python in Science Conference (SciPy2008). Pasadena, CA USA, pp. 11–15.
Harris, P.M., 2010. Delineating and quantifying depositional facies patterns in carbonate reservoirs: Insight from modern analogs. AAPG Bull. 94, 61–86. http://dx.doi.org/10.1306/07060909014.
Hartley, A., Weissmann, G., Nichols, G., Warwick, G., 2010. Large distributive fluvial systems: characteristics, distribution, and controls on development. J. Sediment. Res. 80, 167–183.
Haunert, J.-H., Sester, M., 2008. Area collapse and road centerlines based on Straight Skeletons. GeoInformatica 12, 169–191.
Holzweber, B., Hartley, A., Weissmann, G., 2014. Scale invariance in fluvial barforms: implications for interpretation of fluvial systems in the rock record. Pet. Geosci. 20, 221–224.
Howell, J., Skorstad, A., MacDonald, A., Fordham, A., Flint, S., Fjellvoll, B., Manzocchi, T., 2008. Sedimentological parameterization of shallow-marine reservoirs. Pet. Geosci. 14, 17–34.
Howell, J.A., Martinius, A.W., Good, T.R., 2014. The application of outcrop analogues in geological modelling: a review, present status and future outlook. In: Martinius, A.W., Howell, J.A., Good, T.R. (Eds.), Sediment-Body Geometry an Heterogeneity: Analogue Studies for Modelling the Subsurface, 387. Special Publications, Geological Society, London, pp. 135–151.
Kadima, E., Delvaux, D., Sebagenzi, S.N., Tack, L., Kabeya, S.M., 2011. Structure and geological history of the Congo Basin: an integrated interpretation of gravity, magnetic and reflection seismic data. Basin Res. 23, 499–527.
Kröner, S., Doménech Carbó, M.T., 2013. Determination of minimum pixel resolution for shape analysis: proposal of a new data validation method for computerized images. Powder Technol. 245, 297–313.
Lakshmi, J.K., Punithavalli, M., 2009A Survey on Skeletons in Digital Image Processing. In: 2009 International Conference on Digital Image Processing. pp. 260–269.
Larue, D.K., Legarre, H., 2004. Flow units, connectivity, and reservoir characterization in a wave-dominated deltaic reservoir: Meren reservoir, Nigeria. AAPG Bull. 88, 303–324.
Lisle, R.J., 2006. Google Earth: a new geological resource. Geol. Today 22, 29–32.
Massey, T.A., Fernie, A.J., Ainsworth, R., Nanson, R.A., Vakarelov, B.K., 2014. Detailed mapping, three-dimensional modelling and upscaling of a mixed-influence delta system, Mitchell River delta, Gulf of Carpentaria, Australia. In: Martinius, A.W., Howell, J.A., Good, T.R. (Eds.), Sediment-Body Geometry an Heterogeneity: Analogue Studies for Modelling the Subsurface, 387. Special Publications, Geological Society, London, pp. 135–151.
McAllister, M., Snoeyink, J., 2000. Medial axis generalization of river networks. Cartogr. Geogr. Inf. Sci. 27, 129–138.
Nanson, R., Ainsworth, R., Vakarelov, B., Fernie, J., Massey, A., 2012. Geometric attributes of reservoir elements in a modern, low accommodation, tide-dominated delta. APPEA J., 483–492.
Nanson, R.A., Vakarelov, B.K., Ainsworth, R.B., Williams, F.M., Price, D.M., 2013. Evolution of a Holocene, mixed-process, forced regressive shoreline: the Mitchell River delta, Queensland, Australia. Mar. Geol. 339, 22–43.
Nichols, G.J., Fisher, J.A., 2007. Processes, facies and architecture of fluvial distributary system deposits. Sediment. Geol. 195, 75–90.
Palágyi, K., Tschirren, J., Hoffman, E.A., Sonka, M., 2006. Quantitative analysis of pulmonary airway tree structures. Comput. Biol. Med. 36, 974–996.
Pavelsky, T.M., Smith, L.C., 2008. RivWidth: a software tool for the calculation of river widths from remotely sensed imagery. Geosci. Remote Sens. Lett., IEEE 5, 70–73.
QGIS Development Team, 2014. QGIS geographic information system. Open Source Geospatial Foundation Project.
Rhodes, E.G., 1982. Depositional model for a chenier plain, Gulf of Carpentaria, Australia. Sedimentology 29, 201–221.
Rittersbacher, A., Buckley, S., Howell, J., 2014. Helicopter-based laser scanning: a method for quantitative analysis of large-scale sedimentary architecture. In: Martinius, A.W., Howell, J.A., Good, T.R. (Eds.), Sediment-Body Geometry an Heterogeneity: Analogue Studies for Modelling the Subsurface, 387. Special Publications, Geological Society, London, pp. 135–151.
Shugar, D.H., Clague, J.J., 2011. The sedimentology and geomorphology of rock avalanche deposits on glaciers. Sedimentology 58, 1762–1783.
Stutz, M., Pilkey, O., 2002. Global Distribution and Morphology of Deltaic Barrier Island Systems. J. Coast. Res., 694–707.
Svensson, S., Sanniti di Baja, G., 2003. Simplifying curve skeletons in volume images. Comp. Vis. Image Underst. 90, 242–257.
Tafesse, S., Fernlund, J.M.R., Bergholm, F., 2012. Digital sieving-Matlab based 3-D image analysis. Eng. Geol. 137–138, 74–84.
Tye, R.S., 2004. Geomorphology: an approach to determining subsurface reservoir dimensions. AAPG Bull. 88, 1123–1147.
USGS, 2009. Global Land Survey, 2000, Landsat ETM+. Sioux Falls, South Dakota, USGS.
Vakarelov, B., Ainsworth, R., 2013. A hierarchical approach to architectural classification in marginal-marine systems: bridging the gap between sedimentology and sequence stratigraphy. AAPG Bull. 97, 1121–1161.
van der Werff, H.M.A., van der Meer, F.D., 2008. Shape-based classification of spectrally identical objects. ISPRS J. Photogramm. Remote Sens. 63, 251–258.
Wang, C., Ren, C., Lei, X., Dai, S., 2011. Automatic skeleton generation and character skinning. In: Proceedings of the 2011 IEEE International Symposium on VR Innovation (ISVRI). pp. 299–304.
Weissmann, G.S., Hartley, A.J., Nichols, G.J., Scuderi, L.A., Olson, M., Buehler, H., Banteah, R., 2010. Fluvial form in modern continental sedimentary basins: d istributive fluvial systems. Geology 38, 39–42.